Journal of Nuclear Medicine, published on July 5, 2018 as doi:10.2967/jnumed.118.209155

^{11}C-DPA-713 versus ^{18}F-GE-180: A preclinical comparison of TSPO-PET tracers to visualize acute and chronic neuroinflammation in a mouse model of ischemic stroke

Aisling Chaney[1], Haley C. Cropper[1], Emily M. Johnson[1], Kendra J. Lechtenberg[2], Todd C. Peterson[2], Marc Y. Stevens[1], Marion S. Buckwalter[2,3] and Michelle L. James[1,2]*.

Affiliations:

[1]*Department of Radiology, Stanford University, Stanford CA, 94305, USA*

[2]*Department of Neurology and Neurological Sciences, Stanford University, Stanford CA, 94305, USA*

[3]*Department of Neurosurgery, Stanford University School of Medicine, Stanford, California 94305, USA*

***Corresponding Author**: Michelle James, 1201 Welch Road, P-206
Stanford, CA 94305, USA. V: (650)497-0153; F: (650)724-4948
(mljames@stanford.edu).

First Author: Aisling Chaney (postdoctoral scholar), 1201 Welch Road, P-255,
Stanford, CA 94305. V: (650)721-3324; F: (650)724-4948 (aislingc@stanford.edu).

Running title: Imaging neuroinflammation post-stroke

ABSTRACT

Neuroinflammation plays a key role in neuronal injury following ischemic stroke. Positron emission tomography (PET) imaging of translocator protein 18 kDa (TSPO) permits longitudinal, non-invasive visualization of neuroinflammation in both pre-clinical and clinical settings. Many TSPO tracers have been developed, however it is unclear which tracer is the most sensitive and accurate for monitoring the *in vivo* spatiotemporal dynamics of neuroinflammation across applications. Hence, there is a need for head-to-head comparisons of promising TSPO-PET tracers across different disease states. Accordingly, the aim of this study was to directly compare two promising second-generation TSPO tracers; ^{11}C-DPA-713 and ^{18}F-GE-180, for the first time at acute and chronic time-points following ischemic stroke. **Methods:** Following distal middle cerebral artery occlusion (dMCAO) or sham surgery, mice underwent consecutive PET/CT (computed tomography) imaging with ^{11}C-DPA-713 and ^{18}F-GE-180 at 2, 6, and 28 days after stroke. T2-weighted magnetic resonance (MR) images were acquired to enable delineation of ipsilateral (infarct) and contralateral brain regions of interest (ROIs). PET/CT images were analyzed by calculating % injected dose per gram (%ID/g) in MR-guided ROIs. Standardized uptake value ratios were determined using the contralateral thalamus (SUV_{Th}) as a pseudo-reference region. *Ex vivo* autoradiography and immunohistochemistry were performed to verify *in vivo* findings. **Results:** Significantly increased tracer uptake was observed in the

ipsilateral compared to contralateral ROI (SUV_{Th}, 50-60 min summed data) at acute and chronic time-points using ^{11}C-DPA-713 and ^{18}F-GE-180. *Ex vivo* autoradiography confirmed *in vivo* findings demonstrating increased TSPO-tracer uptake in infarcted versus contralateral brain tissue. Importantly, a significant correlation was identified between microglial/macrophage activation (cluster of differentiation 68 - CD68 immunostaining) and ^{11}C-DPA-713-PET signal, that was not evident with ^{18}F-GE-180. No significant correlations were observed between TSPO-PET and activated astrocytes (glial fibrillary acidic protein - GFAP immunostaining). **Conclusion:** ^{11}C-DPA-713 and ^{18}F-GE-180-PET enable detection of neuroinflammation at acute and chronic time-points following cerebral ischemia in mice. ^{11}C-DPA-713-PET reflects the extent of microglial activation in infarcted dMCAO mouse brain tissue more accurately compared to ^{18}F-GE-180, and appears to be slightly more sensitive. These results highlight the potential of ^{11}C-DPA-713 for tracking microglial activation *in vivo* after stroke and warrant further investigation in both pre-clinical and clinical settings.

Key words: TSPO, ischemic stroke, neuroinflammation, PET.

Word count: 4997

INTRODUCTION

Neuroinflammation is a potent driver of neuronal damage and degeneration post-ischemic stroke (*1*,*2*). Activation of glia and infiltration of peripheral immune cells into the brain are central to both the detrimental consequences observed in acute phases following stroke, and the neuroprotective effects; contributing to neuronal repair, survival, and damage limitation (*2*). Although the connection between neuroinflammation and ischemic stroke is unrefuted, the *in vivo* spatiotemporal dynamics of specific immune cells, at acute and chronic time-points, in individual stroke patients is poorly understood. Moreover, how these immune signatures relate to clinical outcomes remains unknown.

Investigating the multi-faceted molecular aspects of the innate and adaptive immune response in the central nervous system post-stroke is mostly restricted to *in vitro* post-mortem analyses (e.g., immunological assays). While these techniques continue to provide invaluable insights into the complex neuro-immune interactions following ischemia, they are limited to a single time-point of inquiry, and thus cannot provide *in vivo* longitudinal data needed to elucidate this dynamic process. With increasing evidence linking chronic neuroinflammation to depression, fatigue, and cognitive decline post-stroke (*3*-*5*), there is a growing need to accurately quantify neuroinflammation *in vivo*. Currently, there are no routine *in vivo* methods approved for detecting and monitoring the innate or adaptive immune

cells non-invasively. Therefore, there is a critical need for specific molecular imaging biomarkers to enhance our understanding of the immune response in acute and chronic phases following ischemia. Such imaging biomarkers would afford unique insights into an individual patient's immune signature and help predict clinical outcomes, including risk of post-stroke dementia (*6,7*). Furthermore, *in vivo* tracking of neuroinflammation post-stroke could provide a means to select patients for novel immune-targeted therapeutics, identify appropriate time windows for meaningful intervention, and monitor treatment response, thus expediting development and translation of efficacious therapies.

The translocator protein 18 kDa (TSPO) represents such a biomarker, for which numerous positron emission tomography (PET) radiotracers have been developed. TSPO expression is high in peripheral tissues, including kidneys, lungs, and steroid-associated tissues (e.g. adrenal glands), and low in healthy brain tissue, where it is mainly restricted to microglia, and to a lesser extent astrocytes (*8,9*). Upon injurious pro-inflammatory stimulation, TSPO protein levels markedly increase in activated microglia and infiltrating myeloid cells, providing a valuable imaging biomarker of activated innate immune cells and neuroinflammation (*8,10*). The first TSPO-PET tracer to be widely evaluated for imaging neuroinflammation was ^{11}C-PK11195. Although ^{11}C-PK11195 provided an opportunity to visualize neuroinflammation in living subjects for the first time, it is unfortunately limited

by inadequate brain penetration and high non-specific binding, resulting in low signal-to-background and poor sensitivity (*11*). Numerous second-generation TSPO-PET tracers have been developed to improve these limitations, including ^{11}C-PBR28 (*12*), ^{11}C-DPA-713 (*13*), ^{18}F-DPA-714 (*14*), ^{18}F-PBR06 (*15*), ^{18}F-FEPPA (*16*), ^{11}C-DAA1106 (*17*), and ^{18}F-GE-180 (*18*). Although many have shown increased sensitivity and affinity compared to ^{11}C-PK11195 (*19-22*), no head-to-head studies have been conducted using two second-generation tracers in the context of stroke. Here, we chose two promising second-generation tracers, ^{11}C-DPA-713 and ^{18}F-GE-180 (both reported to have higher sensitivities than ^{11}C-PK11195), and directly compared their sensitivity and accuracy for detecting acute and chronic neuroinflammation in the distal Middle Cerebral Artery Occlusion (dMCAO) mouse model of stroke. As a secondary aim, we investigated the utility of TSPO-PET for quantifying alterations in peripheral inflammatory responses in the spleen.

MATERIALS AND METHODS

Study Design

The dMCAO mouse model of stroke was chosen for this study due to the reproducible, restricted ischemic damage and low mortality rates associated with this surgery (*23*,*24*). Longitudinal TSPO-PET imaging of dMCAO mice has yet to be reported, however elevated TSPO-PET signal peaks between 3 and 11 days post-stroke using other rodent models of ischemia (e.g., MCAO) (*25*-*28*). Consequently, a 6-day time-point was chosen to ensure the presence of elevated TSPO levels. Additionally, 2-day and 28-day time-points were selected to determine whether TSPO-PET could be used to detect acute and chronic inflammation known to occur in this model (Fig. 1A) (*3*). MRI was performed 2 days post-dMCAO, to provide confirmation of stroke and an anatomical reference for PET image analysis, and was followed by sequential *in vivo* ^{11}C-DPA-713 and ^{18}F-GE-180-PET imaging. For all time-points, ^{11}C-DPA-713-PET was performed first, followed by ^{18}F-GE-180-PET after sufficient radioactive decay of carbon-11 (i.e., 10 half-lives). Following TSPO-PET, brain tissues were collected to perform immunohistochemistry (n = 3-5) to investigate the relationship between TSPO-PET signal for each tracer and glial activation. Additionally, *ex vivo* autoradiography (n = 3-5) was performed for each tracer to obtain high spatial resolution images to confirm *in vivo* findings. A small cohort of mice underwent sham surgery (n = 3)

to control for possible inflammatory responses caused by surgery alone and were imaged at either 2 or 6 days.

dMCAO Surgery

Protocols approved by Stanford University's Institutional Animal Care and Use Committee were used for all animal experiments. Surgery via craniotomy and permanent dMCAO was performed as previously outlined on 3 month-old female C57BL/6J mice (*23*). Sham surgery involving craniotomy and manipulation of the meninges (without dMCAO), was also performed. Post-surgery, animals were administered subcutaneous cefazolin, 25 mg/kg (VWR #89149-888) and buprenorphine SR, 1 mg/kg (Zoopharm, Windsor, CO), and were monitored until fully ambulatory.

Radiosynthesis

Radiosynthesis of ^{11}C-DPA-713 and ^{18}F-GE-180 were completed according to standard methods (*13,18*), and formulated in phosphate-buffered saline (0.1 mol/L NaCl, 0.05 mol/L sodium phosphate, pH 7.4), containing 10% ethanol. Both tracers were obtained with high specific radioactivity (^{11}C-DPA-713: 198.9 ± 10.8, ^{18}F-GE-180: 128.2 ± 13.1 GBq/μmol) and radiochemical purity (>99%) (n = 4).

MR Imaging

Three-dimensional axial (coronal) T2-weighted MR images (TE: 33 ms, TR: 2500 ms, 2 averages, 17 slices) were acquired using a millipede quadrature radiofrequency coil on a 7T MRI Varian Magnex Scientific Magnetic Resonance (MR) scanner system as previously reported (*29*).

PET Imaging

Dynamic PET images 2 days and 6 days after dMCAO surgery were acquired over 60 min using a dual microPET/CT scanner (Inveon, Siemens) as previously described (*29*). Static imaging (10 min) was conducted at 50 min post-tracer injection for the 28-day time-point. Each mouse was intravenously injected via tail vein with 7-11.5 MBq of ^{11}C-DPA-713. After a minimum of ten half-lives, the same mice were anesthetized and injected with 5.4-11.8 MBq of ^{18}F-GE-180. Additional blocking studies were conducted at 6-days post-dMCAO. PK11195 (3 mg/kg) was administered intravenously 15 min prior to tracer injection, and dynamic 60 min PET acquisition was performed.

Image Analysis

Image analysis was performed using VivoQuant software (version 3.0, inviCRO) as previously described (*29*). In brief, PET, CT, and MR images were co-registered, and MR-guided ROIs were manually drawn for infarcted/ipsilateral and contralateral tissue (Supplemental Fig. 1A). To permit accurate quantification of PET tracer uptake without using an invasive arterial input function, a suitable internal reference region is required. This region should have low (if any) specific tracer uptake, and the signal should not differ between study groups/areas of interest. Although TSPO levels are low in healthy brain, no region is truly devoid of TSPO expression, hence a brain reference region should be referred to as a pseudo-reference region. Here, a split-brain atlas was used to quantify tracer uptake in brain structures in left versus right hemispheres in an unbiased manner, which revealed the contralateral thalamus as a pseudo-reference region due to its low TSPO-PET signal that did not vary from uptake in the ipsilateral thalamus (Supplemental Fig. 1B-C). SUV_{Th} were calculated by dividing the ROI (i.e. infarct or contralateral) uptake by that of the contralateral thalamus. Since clinical TSPO-PET stroke studies utilize the ipsilateral cerebellum as a reference region (*30*), the suitability of this structure as a clinically relevant reference region was also assessed (by calculating SUV_{Cb} ratios) (Supplemental Fig. 2). Tracer uptake in the spleen was also quantified to assess peripheral inflammation using both the CT and

PET images for guidance, ensuring no overlap with kidney uptake. IRW was used for PET image visualization.

Autoradiography

Ex vivo autoradiography was performed using previously reported methods (*29*). Briefly, 20 μm-thick brain sections were collected 30 min post-injection of 26.6-71.8 MBq of ^{11}C-DPA-713 and 50 min post-injection of 23-40.5 MBq of ^{18}F-GE-180 at all time-points post-dMCAO. After exposing tissues to digital autoradiography films for 10 half-lives, each film was scanned using a typhoon phosphorimager. ImageJ software version 2.0.0 was used to quantify ipsilateral-to-contralateral uptake ratios to account for any differences in radioactivity injected between tracers.

Immunohistochemistry Staining and Quantitation

For semi-quantitative evaluation of microgliosis and astrogliosis, CD68 and GFAP staining were performed respectively, using previously described methods (*31*). Images were captured in the infarct border and contralateral cortex at 20X via a Nanozoomer 2.0-RS (Hamamatsu) using five sections spaced 480 μm apart per mouse. Blinded, unbiased quantification of area covered by staining in these images was performed using ImageJ software. Immunofluorescent TSPO/CD68 and

TSPO/GFAP double staining was performed, as previously described (*32*), on dMCAO mice 6-day tissue to assess the extent of TSPO-positive microglia versus astrocytes underlying the TSPO-PET signal.

Statistics

GraphPad Prism (version 7) was used for statistical analyses of the data using t-tests, one-way analysis of variance (ANOVA) and two-way ANOVAs with multiple comparisons. A p-value of 0.05 or less was considered significant.

RESULTS

To directly assess the sensitivity of ^{11}C-DPA-713 versus ^{18}F-GE-180, a head-to-head comparison was conducted via sequential PET imaging of the same mice at acute (2 and 6-day) or chronic (28-day) time-points post-stroke. Time activity curves at 2 days post-dMCAO demonstrated small differences in ipsilateral compared to contralateral brain ROI uptake (%ID/g) with significantly higher uptake seen at 55-60 min with ^{11}C-DPA-713, but not with ^{18}F-GE-180 (Fig. 1B). At 6 days, there was markedly increased uptake in the ipsilateral compared to the contralateral ROI for both tracers. Since the highest signal-to-background ratios were observed at 50-60 min post-injection, this time-point was chosen for quantification and subsequent static acquisitions at 28 days.

Summed 50-60 min PET/CT images showed increased tracer uptake in the ipsilateral hemisphere at both acute and chronic time-points (Fig. 2). Quantification revealed a significant increase in tracer uptake (SUV_{Th}) in the ipsilateral compared to the contralateral ROI at 2 days post-dMCAO using ^{11}C-DPA-713 (1.20 ± 0.06 vs 0.98 ± 0.05, $p < 0.05$, $n = 7$) but not ^{18}F-GE-180 (1.01 ± 0.96 vs 0.92 ± 0.42, $p > 0.50$, $n = 7$) (Fig. 3A). Significantly increased ipsilateral uptake was observed for ^{11}C-DPA-713 and ^{18}F-GE-180 at 6 days (^{11}C-DPA-713; 2.11 ± 0.29 vs 0.96 ± 0.08, $p < 0.01$, ^{18}F-GE-180; 2.12 ± 0.26 vs 1.03 ± 0.06, $p < 0.01$). Increased ipsilateral uptake was maintained for both tracers at 28 days post-dMCAO (^{11}C-DPA-713; 1.49 ± 0.04 vs 0.89 ± 0.04, $p < 0.0001$, ^{18}F-GE-180; 1.59 ± 0.07 vs 0.97 ± 0.03, $p < 0.0001$). Conversely, low brain uptake was observed for sham mice (2 and 6 days post-surgery, Supplemental Fig. 4, Fig. 3A), with no significant differences between ipsilateral and contralateral ROI uptake observed for either tracer. The ratio of ipsilateral-to-contralateral uptake at 2, 6, and 28 days post-dMCAO did not differ significantly between tracers (Fig. 3B). Similar findings were observed when using the ipsilateral cerebellum as a pseudo-reference region (SUV_{Cb}) (Supplemental Fig. 2). Blocking with PK11195 at 6 days post-dMCAO revealed a significant decrease in TSPO-PET signal in the infarct ROI of dMCAO mice using both ^{11}C-DPA-713 and ^{18}F-GE-180, confirming specificity of these tracers (Supplemental Fig. 3).

Quantification of spleen uptake revealed significant increases for both tracers from 2 to 6 days post-stroke (^{11}C-DPA-713; 7.68 ± 1.84 vs 12.25 ± 3.65 %ID/g, ^{18}F-GE-180; 12.57 ± 1.11 vs 14.16 ± 3.12 %ID/g) (Supplemental Fig. 5). Additionally, a significant increase was observed between 6 and 28 days with ^{18}F-GE-180 (14.16 ± 3.12 vs 20.19 ± 4.3 %ID/g), but not with ^{11}C-DPA-713. No correlation was observed between tracer uptake in the spleen and the infarct ROI.

Ex vivo digital autoradiography results support *in vivo* PET findings with increased tracer uptake seen in the ipsilateral compared to contralateral hemisphere (Fig. 4A). Ipsilateral-to-contralateral ratios were greater than one for both tracers at all time-points, indicating increased binding in infarcted tissue (Fig. 4B). In line with *in vivo* findings, ipsilateral-to-contralateral ratios did not differ significantly between tracers at any time-point.

CD68 immunostaining of brain tissue, reflecting activated microglia/macrophages, corresponded well with PET and autoradiography results (Fig. 5). Quantification revealed markedly elevated levels of CD68 staining in the ipsilateral (infarct border) compared to contralateral brain tissue of dMCAO mice (Fig. 5B, 2 days; 8.95 ± 1.65 vs 1.05 ± 0.37, $p = 0.0084$, $n = 4$, 6 days; 14.47 ± 6.69 vs 0.69 ± 0.03, $p < 0.0001$, $n = 4$, 28 days; 15.76 ± 5.13 vs 0.54 ± 0.42, $p < 0.0001$, $n = 5$), whereas low levels of staining were observed in 6-day sham mice (1.20 ± 1.19 vs 0.50 ± 0.29, $p = 0.998$, $n = 3$). Similarly, GFAP levels were significantly

elevated in ipsilateral versus contralateral tissue of dMCAO (Fig. 6, 2 days; 15.61 ± 5.80 vs 0.46 ± 0.37, p = 0.0001, n = 4, 6 days; 19.83 ± 4.67 vs 0.71 ± 0.87, p < 0.0001, n = 4, 28 days; 32.97 ± 8.00 vs 0.25 ± 0.16, p < 0.0001, n = 5) but not sham mice. *In vivo* ^{11}C-DPA-713-PET signal significantly correlated with *ex vivo* CD68 levels (Fig. 7A, r = 0.603, p = 0.017, n = 15), whereas no significant correlation was observed with ^{18}F-GE-180 (Fig. 7B). GFAP levels did not correlate with the *in vivo* TSPO-PET signal from either tracer (Fig. 7C-D). These results were supported by co-localization of TSPO and CD68 expression in the infarct of 6-day dMCAO mice. TSPO immunofluorescence staining was not observed on GFAP-positive cells (Supplemental Fig. 6).

DISCUSSION

Here, we report the first head-to-head comparison of two promising second-generation TSPO tracers, ^{11}C-DPA-713 and ^{18}F-GE-180, in a rodent model of cerebral ischemia. The overall goal was to evaluate the sensitivity and accuracy of these tracers at both acute and chronic time-points following dMCAO surgery.

Here, we prove TSPO-PET is a valuable tool for detecting acute and chronic neuroinflammation in cerebral ischemia. ^{11}C-DPA-713 appeared to be more sensitive than ^{18}F-GE-180, with successful delineation of neuroinflammation in the infarcted ROI at 2 days post-dMCAO, when ^{18}F-GE-180 did not detect a significant

difference. These results are consistent with previous reports demonstrating the high sensitivity of ^{11}C-DPA-713 to detect subtle inflammatory changes, with a recent study demonstrating significant increases in ^{11}C-DPA-713 uptake with normal aging that was not evident with ^{11}C-PK11195 and has only previously been identifiable via *ex vivo* means. Both tracers effectively identified inflammation in the ipsilateral ROI at 6 and 28 days post-dMCAO, highlighting the potential of TSPO-PET for quantifying and tracking chronic inflammation post-stroke. Similar results were found using SUV_{Cb}, indicating the translational potential of these tracers for imaging stroke patients. Additionally, pre-blocking with cold PK11195 revealed significantly decreased binding of both tracers in dMCAO mice at 6-days post-stroke, confirming the specificity of both tracers for TSPO.

In vivo PET results were validated by *ex vivo* autoradiography and immunostaining of activated microglia/macrophages and astrocytes. Autoradiography confirmed increased tracer uptake in infarcted tissue for both tracers at all time-points. Ipsilateral-to-contralateral ratios for ^{18}F-GE-180 and ^{11}C-DPA-713 obtained with autoradiography were slightly different to those observed with PET. Notably, a slightly higher ratio was seen with ^{18}F-GE-180 autoradiography at 2 days. A possible explanation for the lack of discrimination using *in vivo* ^{18}F-GE-180-PET at this time-point may be the limited resolution of the PET scanner to detect this difference, or the increased blood pool concentration

of ^{18}F-GE-180 resulting in reduced signal-to-background masking differential uptake.

Increased ipsilateral TSPO-PET signal was supported by striking increases in CD68 immunostaining in the ipsilateral infarct border. Moreover, correlation of *in vivo* PET and *ex vivo* immunostaining of tissues from the same animals revealed novel insights into the comparative specificity of these tracers. ^{11}C-DPA-713-PET signal correlated significantly with *ex vivo* levels of activated microglia/macrophages. Surprisingly, this was not observed with ^{18}F-GE-180, indicating that ^{11}C-DPA-713-PET more accurately depicts microglial activation. No correlation was found between TSPO-PET and GFAP expression, suggesting that in the context of stroke, the TSPO-PET signal mainly represents activated microglia/macrophages. This is in line with our findings demonstrating TSPO expression in the infarct core and border co-localizes almost exclusively with CD68, and agrees with results from a previous study using MCAO rats (*28*).

Our findings are consistent with previous reports in different rodent models of stroke demonstrating increased ipsilateral uptake using TSPO-PET (*19,21,25-28*). However, few head-to-head studies have been conducted to date, and none have compared two second-generation TSPO tracers in stroke models. Enhanced sensitivity has previously been demonstrated with ^{18}F-DPA-714 (*19*) and ^{18}F-GE-180 versus ^{11}C-PK11195 using the MCAO rat model (*21*). Additionally, ^{18}F-DPA-

714 has been shown to perform better *in vivo,* displaying a higher ipsilateral to contralateral ratio compared to both ^{11}C-PK11195 and ^{11}C-DPA-713 in a rat model of AMPA-induced unilateral neuroinflammation (*20*). Yet, increased ipsilateral-to-contralateral ratios were observed with ^{18}F-GE-180-PET when compared to ^{11}C-PK11195, which were not evident with ^{18}F-DPA-714 using a similar model of unilateral neuroinflammation (*22*). However, ^{18}F-GE-180 and ^{18}F-DPA-714 imaging in these studies was conducted using separate cohorts and therefore did not directly compare tracers. The discrepancies between these studies highlights the need for direct head-to-head comparison studies in reproducible models of neuroinflammation, and emphasizes the importance of the current study, which will help guide future experimental design for investigating neuroinflammation post-stroke.

The current work reveals novel insights into the temporal dynamics of neuroinflammation post-stroke. Previous studies have reported increased TSPO-PET binding in ROIs encompassing infarcted tissue ranging from 3 to 21 days post-insult (*19,21,25-28*). However, these studies did not detect increased ipsilateral inflammation as early as 2 days post-stroke, as demonstrated here with ^{11}C-DPA-713. Moreover, few studies have investigated the effect of chronic inflammation post-stroke. A study by Walberer *et al.,* using ^{11}C-PK11195 in a rat model of ischemia demonstrated the highly dynamic process of inflammation with peak ^{11}C-PK11195 binding occurring in the infarct at 7 days and spreading to thalamic

regions detectable as far as 7 months following stroke (*33*). Similarly, Walter *et al.,* found that neuroinflammation spread to surrounding subcortical areas at 4 and 8 weeks post-permanent MCAO using ^{11}C-PK11195 (*34*). These results indicate a local versus remote microglial activation phenomena which warrants further investigation using more sensitive tracers.

Since the spleen is central to the activation, proliferation, and trafficking of immune cells to the site of injury in the early stages following stroke (*35*), we quantified spleen PET signal and found a stepwise increase in TSPO binding post-dMCAO. Although this increase did not correlate with brain inflammation, it highlights the importance of the dynamic changes occurring in the periphery post-stroke and demonstrates the benefits of using full body TPSO-PET to investigate these processes. To our knowledge, this is the first investigation of peripheral TSPO-PET in stroke.

CONCLUSION

Here we present the first head-to-head comparison of two second-generation TSPO-PET tracers in a rodent model of ischemic stroke. Both tracers enabled identification of acute and chronic inflammation in infarcted brain tissue, however ^{11}C-DPA-713-PET more accurately reflected microglial/macrophage activation and afforded earlier detection compared to ^{18}F-GE-180. Results from this study highlight the utility of TSPO-PET as an invaluable tool for deciphering the

in vivo role of neuroinflammation in both early and late stages post-stroke in the central nervous system and periphery. Future work will focus on investigating the relationship between TSPO-PET signal, neurological symptoms, and long-term outcomes in rodent models and stroke patients.

Funding

This project was funded partly by a "Big Ideas in Neuroscience" grant from the Stanford Neurosciences Institute to the Stroke Collaborative Action Network (Buckwalter).

ACKNOWLEDGEMENTS

We are grateful for the support from the SCi3 small animal imaging facility at Stanford. We also thank InviCRO for their assistance with VivoQuant software, and the Radiochemistry Facility, especially Dr. Jun Park.

REFERENCES

1. Kim JY, Kawabori M, Yenari MA. Innate inflammatory responses in stroke: mechanisms and potential therapeutic targets. *Curr Med Chem.* 2014;21:2076-2097.

2. Jin R, Liu L, Zhang S, Nanda A, Li G. Role of inflammation and its mediators in acute ischemic stroke. *J Cardiovasc Transl Res.* 2013;6:834-851.

3. Doyle KP, Quach LN, Sole M, et al. B-lymphocyte-mediated delayed cognitive impairment following stroke. *J Neurosci.* 2015;35:2133-2145.

4. Becker KJ, Tanzi P, Zierath D, Buckwalter MS. Antibodies to myelin basic protein are associated with cognitive decline after stroke. *J Neuroimmunol.* 2016;295-296:9-11.

5. Becker KJ, Buckwalter MS. Stroke, Inflammation and the immune response: dawn of a new era. *Neurotherapeutics.* 2016;13:659-660.

6. Kalaria RN, Akinyemi R, Ihara M. Stroke injury, cognitive impairment and vascular dementia. *Biochim Biophys Acta.* 2016;1862:915-925.

7. Pendlebury ST, Rothwell PM. Prevalence, incidence, and factors associated with pre-stroke and post-stroke dementia: a systematic review and meta-analysis. *Lancet Neurol.* 2009;8:1006-1018.

8. Scarf AM, Kassiou M. The translocator protein. *J Nucl Med.* 2011;52:677-680.

9. Fan J, Lindemann P, Feuilloley MG, Papadopoulos V. Structural and functional evolution of the translocator protein (18 kDa). *Curr Mol Med.* 2012;12:369-386.

10. Papadopoulos V, Lecanu L. Translocator protein (18 kDa) TSPO: an emerging therapeutic target in neurotrauma. *Exp Neurol.* 2009;219:53-57.

11. Varrone A, Lammertsma AA. Imaging of neuroinflammation: TSPO and beyond. *Clin Transl Imaging.* 2015;3:389-390.

12. Imaizumi M, Kim HJ, Zoghbi SS, et al. PET imaging with [11C]PBR28 can localize and quantify upregulated peripheral benzodiazepine receptors associated with cerebral ischemia in rat. *Neurosci Lett.* 2007;411:200-205.

13. James ML, Fulton RR, Henderson DJ, et al. Synthesis and in vivo evaluation of a novel peripheral benzodiazepine receptor PET radioligand. *Bioorg Med Chem.* 2005;13:6188-6194.

14. James ML, Fulton RR, Vercoullie J, et al. DPA-714, a new translocator protein-specific ligand: synthesis, radiofluorination, and pharmacologic characterization. *J Nucl Med.* 2008;49:814-822.

15. Imaizumi M, Briard E, Zoghbi SS, et al. Kinetic evaluation in nonhuman primates of two new PET ligands for peripheral benzodiazepine receptors in brain. *Synapse.* 2007;61:595-605.

16. Wilson AA, Garcia A, Parkes J, et al. Radiosynthesis and initial evaluation of [18F]-FEPPA for PET imaging of peripheral benzodiazepine receptors. *Nucl Med Biol.* 2008;35:305-314.

17. Maeda J, Suhara T, Zhang MR, et al. Novel peripheral benzodiazepine receptor ligand [11C]DAA1106 for PET: an imaging tool for glial cells in the brain. *Synapse.* 2004;52:283-291.

18. Wadsworth H, Jones PA, Chau WF, et al. [(1)(8)F]GE-180: a novel fluorine-18 labelled PET tracer for imaging Translocator protein 18 kDa (TSPO). *Bioorg Med Chem Lett.* 2012;22:1308-1313.

19. Boutin H, Prenant C, Maroy R, et al. [18F]DPA-714: direct comparison with [11C]PK11195 in a model of cerebral ischemia in rats. *PLoS One.* 2013;8:e56441.

20. Chauveau F, Van Camp N, Dolle F, et al. Comparative evaluation of the translocator protein radioligands 11C-DPA-713, 18F-DPA-714, and 11C-PK11195 in a rat model of acute neuroinflammation. *J Nucl Med.* 2009;50:468-476.

21. Boutin H, Murray K, Pradillo J, et al. (18)F-GE-180: a novel TSPO radiotracer compared to (11)C-R-PK11195 in a preclinical model of stroke. *Eur J Nucl Med Mol Imaging.* 2015;42:503-511.

22. Sridharan S, Lepelletier FX, Trigg W, et al. Comparative Evaluation of Three TSPO PET Radiotracers in a LPS-Induced Model of Mild Neuroinflammation in Rats. *Mol Imaging Biol.* 2017;19:77-89.

23. Doyle KP, Buckwalter MS. A mouse model of permanent focal ischemia: distal middle cerebral artery occlusion. *Methods Mol Biol.* 2014;1135:103-110.

24. Doyle KP, Fathali N, Siddiqui MR, Buckwalter MS. Distal hypoxic stroke: a new mouse model of stroke with high throughput, low variability and a quantifiable functional deficit. *J Neurosci Methods.* 2012;207:31-40.

25. Domercq M, Szczupak B, Gejo J, et al. PET Imaging with [(18)F]FSPG Evidences the Role of System xc(-) on Brain Inflammation Following Cerebral Ischemia in Rats. *Theranostics.* 2016;6:1753-1767.

26. Toth M, Little P, Arnberg F, et al. Acute neuroinflammation in a clinically relevant focal cortical ischemic stroke model in rat: longitudinal positron emission tomography and immunofluorescent tracking. *Brain Struct Funct.* 2016;221:1279-1290.

27. Lartey FM, Ahn GO, Shen B, et al. PET imaging of stroke-induced neuroinflammation in mice using [18F]PBR06. *Mol Imaging Biol.* 2014;16:109-117.

28. Martin A, Boisgard R, Theze B, et al. Evaluation of the PBR/TSPO radioligand [(18)F]DPA-714 in a rat model of focal cerebral ischemia. *J Cereb Blood Flow Metab.* 2010;30:230-241.

29. Chaney A, Johnson EJ, Cropper HC, James ML. PET Imaging of Neuroinflammation Using [11C]DPA-713 in a Mouse Model of Ischemic Stroke. *JoVE.* 2018.

30. Gerhard A, Schwarz J, Myers R, Wise R, Banati RB. Evolution of microglial activation in patients after ischemic stroke: a [11C](R)-PK11195 PET study. *Neuroimage.* 2005;24:591-595.

31. Cekanaviciute E, Fathali N, Doyle KP, Williams AM, Han J, Buckwalter MS. Astrocytic transforming growth factor-beta signaling reduces subacute neuroinflammation after stroke in mice. *Glia.* 2014;62:1227-1240.

32. Chaney A, Bauer M, Bochicchio D, et al. Longitudinal investigation of neuroinflammation and metabolite profiles in the APPswe xPS1Deltae9 transgenic mouse model of Alzheimer's disease. *J Neurochem.* 2018;144:318-335.

33. Walberer M, Jantzen SU, Backes H, et al. In-vivo detection of inflammation and neurodegeneration in the chronic phase after permanent embolic stroke in rats. *Brain Res.* 2014;1581:80-88.

34. Walter HL, Walberer M, Rueger MA, et al. In vivo analysis of neuroinflammation in the late chronic phase after experimental stroke. *Neuroscience.* 2015;292:71-80.

35. Liu ZJ, Chen C, Li FW, et al. Splenic responses in ischemic stroke: new insights into stroke pathology. *CNS Neurosci Ther.* 2015;21:320-326.

FIGURES

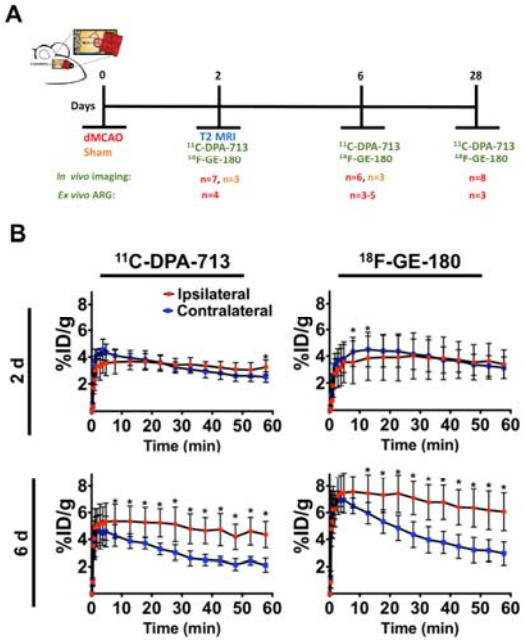

FIGURE 1. Study design timeline adapted from Doyle *et al. (23)* (A). Time activity curves depicting dynamic ^{11}C-DPA-713 and ^{18}F-GE180 uptake (%ID/g) in ipsilateral and contralateral brain ROIs at 2 and 6 days post-dMCAO surgery (mean ± SD) (B). Wilcoxon matched paired test (*$p < 0.05$).

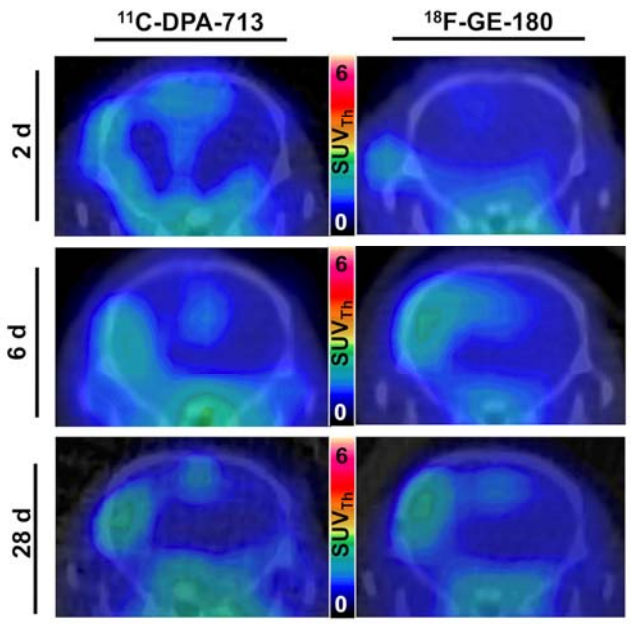

FIGURE 2. Representative ^{11}C-DPA-713 and ^{18}F-GE180 PET/CT coronal mouse brain images of dMCAO mice (SUV_{Th}).

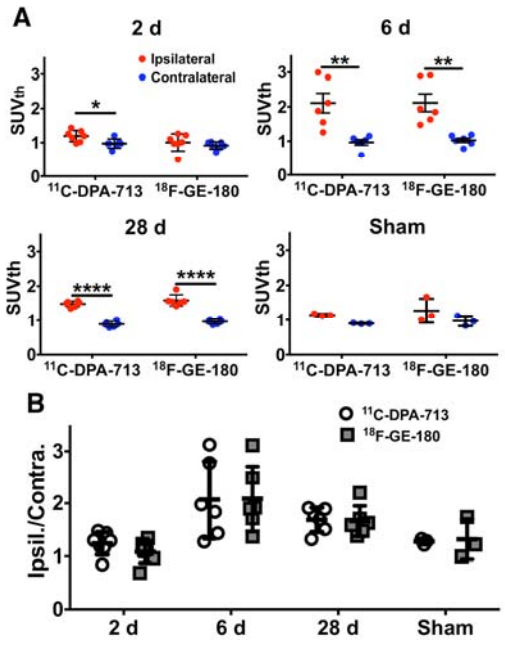

FIGURE 3. PET image quantification of ^{11}C-DPA-713 and ^{18}F-GE-180 uptake (SUV_{Th}) in ipsilateral and contralateral ROIs in dMCAO mice at 2, 6 and 28 days and sham mice at 6 days post-surgery (mean ± SD) (A). Ipsilateral to contralateral uptake ratios in dMCAO and sham mice (mean ± SD) (B). Two-way ANOVA, Sidak's post-hoc test (*$p < 0.05$, **$p < 0.01$, ****$p < 0.0001$).

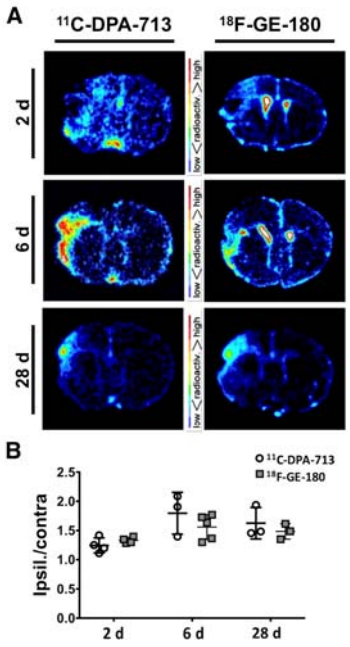

FIGURE 4. Representative *ex vivo* coronal brain autoradiography images of ^{11}C-DPA-713 and ^{18}F-GE-180 uptake at 2, 6, and 28 days post-dMCAO surgery (A). Ratios of mean pixel intensity in ipsilateral versus contralateral brain ROIs for ^{11}C-DPA-713 and ^{18}F-GE-180 autoradiography (mean ± SD) (B).

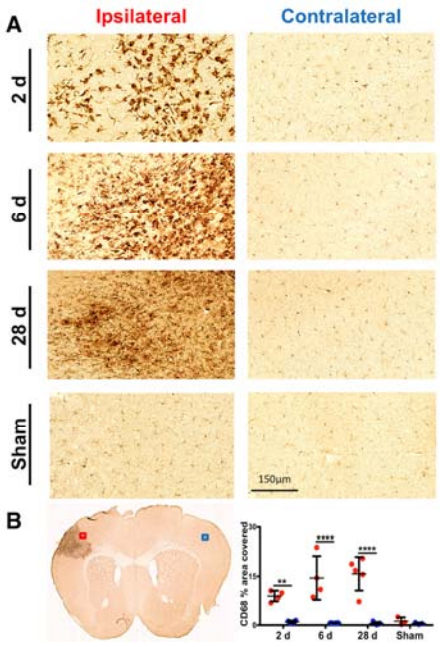

FIGURE 5. Representative images of CD68 immunostaining in ipsilateral infarct border versus contralateral brain tissue after dMCAO and sham surgery (20x magnification) (A). Representative 6-day dMCAO brain section and quantification of the percentage area covered with CD68 staining (mean ± SD) in the ipsilateral (ROI indicated by red box) and contralateral (ROI indicated by blue box) tissue of dMCAO and sham animals (B). Two-way ANOVA, Sidak's post-hoc tests (**$p < 0.01$, ****$p < 0.0001$).

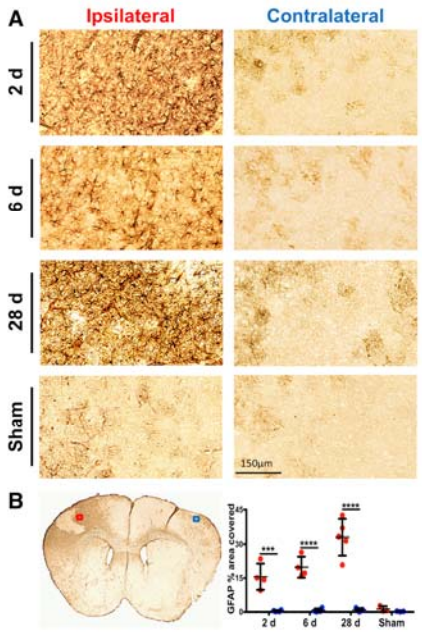

FIGURE 6. Representative images of GFAP immunostaining in ipsilateral infarct border versus contralateral brain tissue after dMCAO and sham surgery (20x magnification) (A). Representative 6-day dMCAO brain section and quantitation of the percentage area covered with GFAP staining (mean ± SD) in the ipsilateral (ROI indicated by red box) and contralateral (ROI indicated by blue box) tissue of dMCAO and sham animals (B). Two-way ANOVA, Sidak's post-hoc tests (***$p < 0.001$, ****$p < 0.0001$).

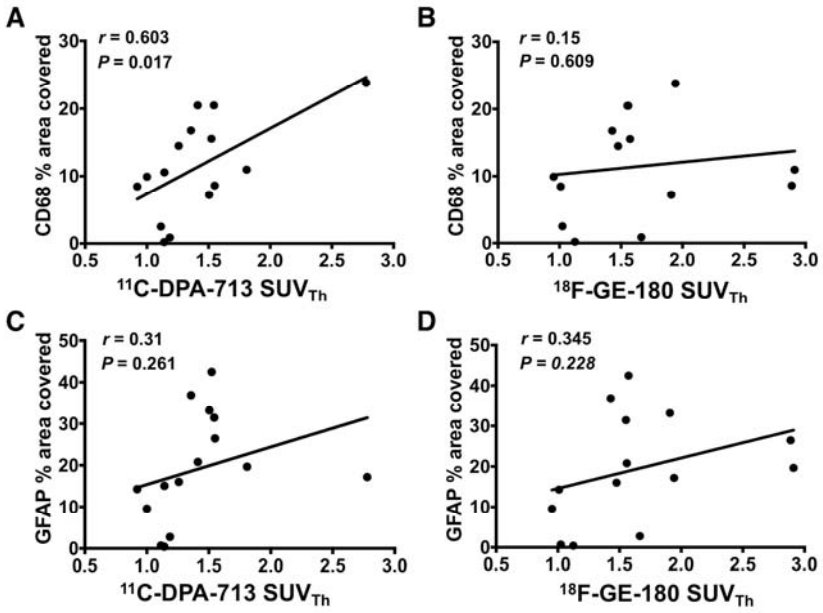

FIGURE 7. Correlation between *in vivo* ^{11}C-DPA-713 and ^{18}F-GE-180 signal (SUV_{Th}) and *ex vivo* CD68 (microglia/macrophage) and GFAP (astrocyte) immunostaining across all groups (^{11}C-DPA-713: day-2; n = 3, day-6; n = 4, day-28; n = 4, sham n = 3, ^{18}F-GE-180: day-2; n = 2, day-6 n = 4, day-28 n = 4, sham; n = 3). Pearson's correlation.

Supplementary Data

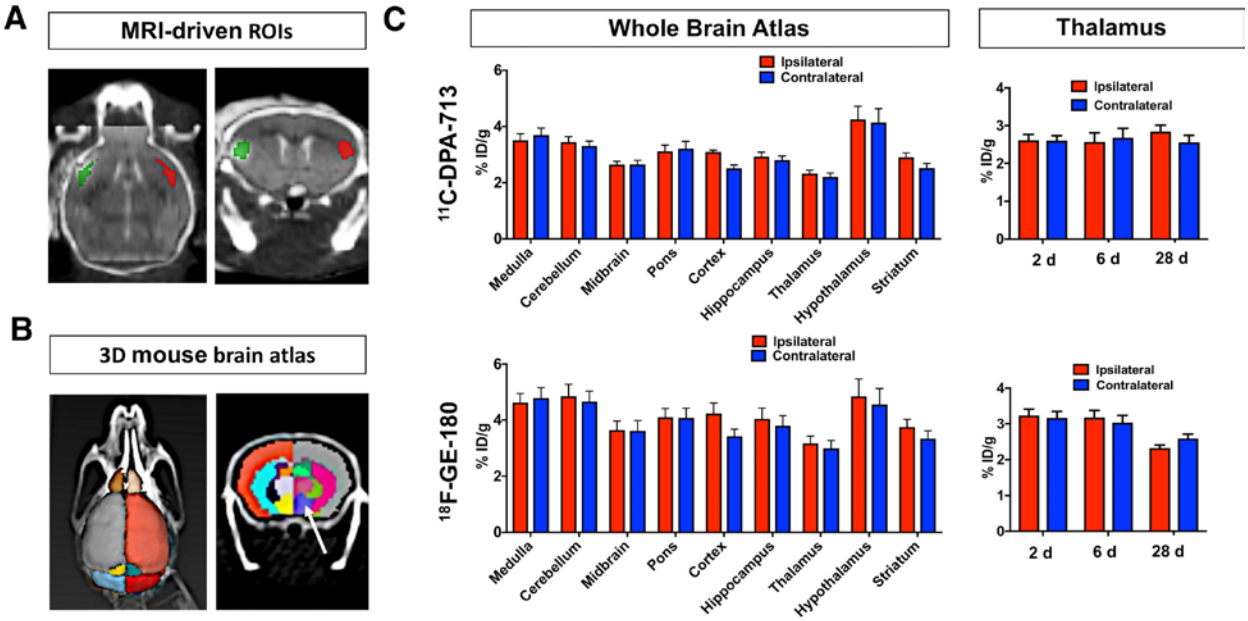

Supplementary Figure 1. MRI-driven ROI analysis (A). 3D mouse brain atlas analysis (B). Results from whole brain atlas revealed the contralateral thalamus as a suitable pseudo-reference region (C).

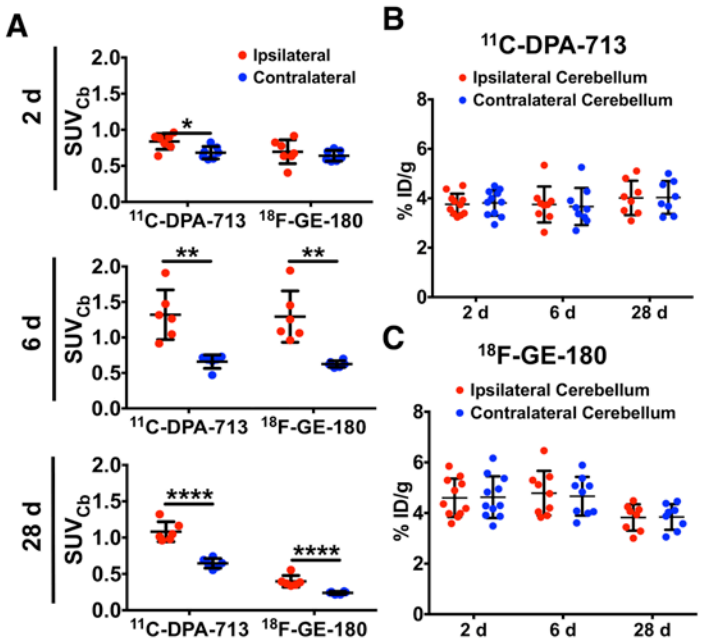

Supplementary Figure 2. PET image quantification of ^{11}C-DPA-713 and ^{18}F-GE-180 uptake in dMCAO mice using the ipsilateral cerebellum (SUV_{Cb}) (A). ^{11}C-DPA-713 (B) and ^{18}F-GE-180 (C) uptake in the ipsilateral and contralateral cerebellum did not differ in dMCAO mice over time.

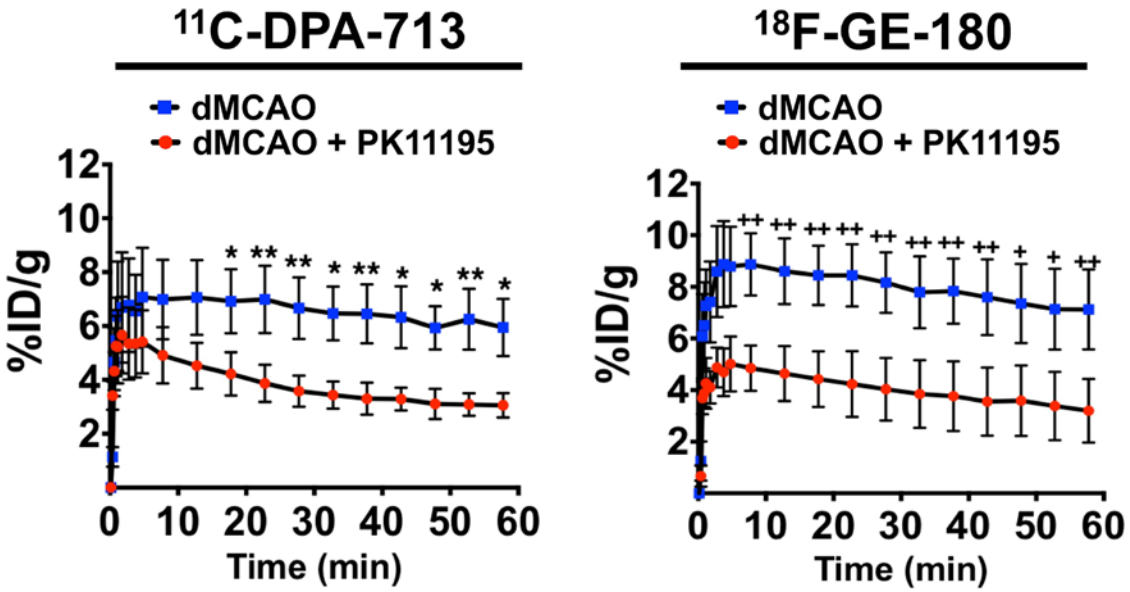

Supplementary Figure 3. Time activity curves depicting tracer uptake in the infarct of dMCAO mice with and without pre-blocking with PK11195 (3mg/kg) at 6 days post-stroke (mean ± SD). Wilcoxon matched paired test (*p<0.05, **p<0.01, +p<0.001, ++p<0.0001).

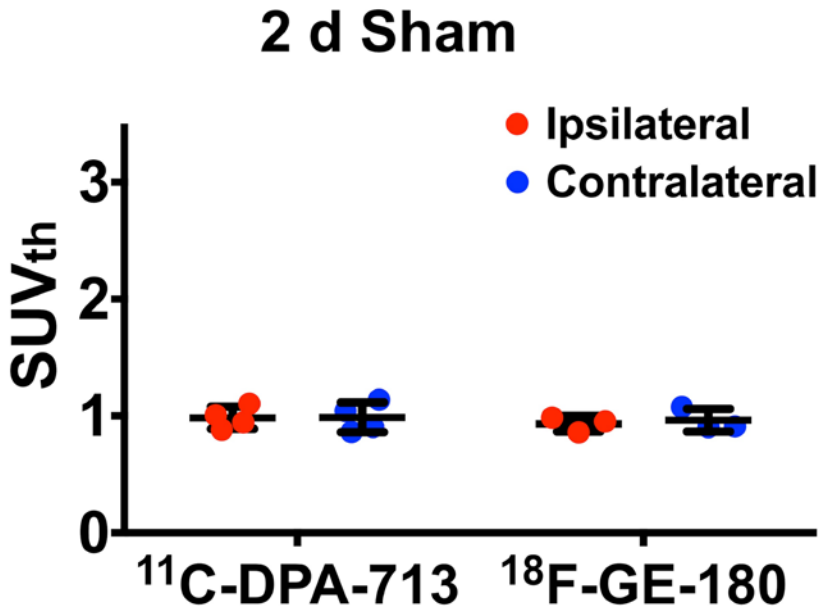

Supplementary Figure 4. ^{11}C-DPA-713 and ^{18}F-GE-180 uptake (SUV_{Th}) in ipsilateral and contralateral ROIs in sham mice 2 days post-surgery (mean ± SD).

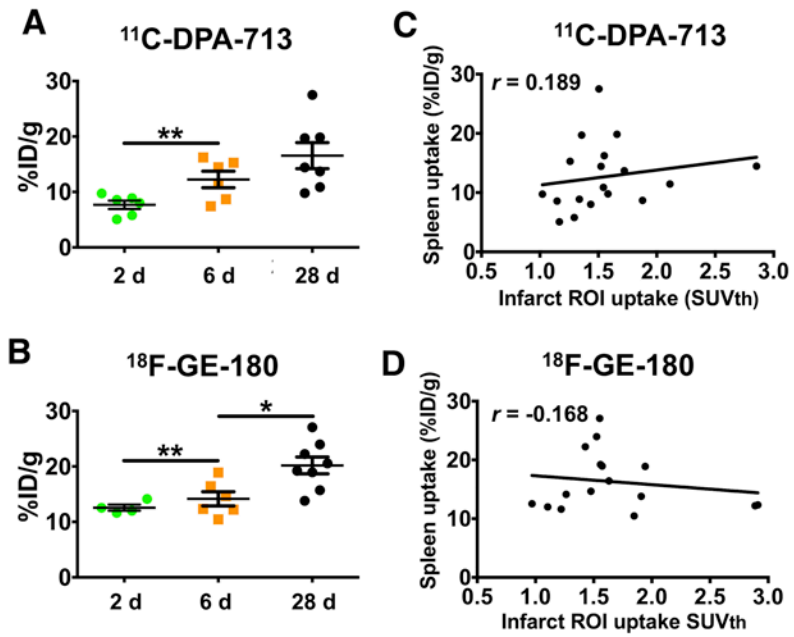

Supplementary Figure 5. ^{11}C-DPA-713 and ^{18}F-GE-180 spleen uptake (%ID/g) (A, B). Relationship between spleen uptake (%ID/g) and infarct uptake (SUV_{Th}) using Pearson's correlation for ^{11}C-DPA-713 (C) and ^{18}F-GE-180 (D).

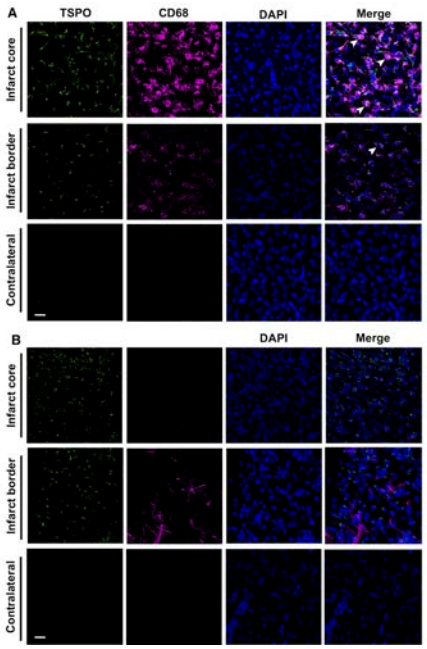

Supplementary Figure 6. Immunofluorescent TSPO/CD68 (A) and TSPO/GFAP (B) double staining depicting that expression of TSPO is primarily in CD68-positive but not GFAP-positive cells at 6 days post-dMCAO.